Absolute absorption spectroscopy based on molecule interferometry

Stefan Nimmrichter,[1] Klaus Hornberger,[2] Hendrik Ulbricht,[1] and Markus Arndt[1]

[1]*Faculty of Physics, University of Vienna, Boltzmanngasse 5, 1090 Vienna, Austria*

[2]*Arnold Sommerfeld Center for Theoretical Physics, Ludwig-Maximilians-Universität München, Theresienstraße 37,*

80333 Munich, Germany

We propose a method to measure the absolute photon absorption cross section of neutral molecules in a molecular beam. It is independent of our knowledge of the particle beam density, nor does it rely on photo-induced fragmentation or ionization. The method is based on resolving the recoil resulting from photon absorption by means of near-field matter-wave interference, and it thus applies even to very dilute beams with low optical densities. Our discussion includes the possibility of internal state conversion as well as fluorescence. We assess the influence of various experimental uncertainties and show that the measurement of absolute absorption cross sections is conceivable with high precision and using existing technologies.

I. INTRODUCTION

Optical spectroscopy is a key technology for unraveling electronic, vibrational, rotational, and structural properties of atoms, molecules, and clusters with applications in physics, astronomy, chemistry, and biology. Specifically, their absorption cross sections are nowadays routinely measured with commercial spectrometers, using a large number of precise and sensitive methods covered in modern textbooks [1–3]. A general interest in these applications is to improve the spectral resolution, the sensitivity to small sample quantities, and the precision with regard to the absolute magnitude of the absorption cross section.

In the present article, we propose a method for determining the absolute value of the absorption cross section of neutral nanoparticles at a given optical frequency. In molecular or cluster beam physics this is usually a nontrivial task: Although absolute absorption coefficients can be measured rather precisely even at low densities, the extraction of absorption cross sections is often limited to volatile substances, whose pressure and number density can be determined with sufficient accuracy [4,5]. For complex nanoparticles, information about the particle number is often only available with low precision. Instead, some experiments occasionally use information about the absorption cross section to characterize the supersonic beam composition [6]. Even for effusive beams, which are better controlled and understood, inaccuracies in measuring the source pressure often lead to a large error in the derived optical cross section [7,8].

In all these cases, optical spectra may still be recorded with very high spectral resolution using established methods, yet to properly normalize the entire spectrum it remains important to determine the absolute absorption cross section at least at one anchor point, i.e., at a single wavelength. Such a measurement of an absolute cross section can be achieved by referencing the absorption to a different signal that is derived from the same molecular beam. In the past, various such *in situ* normalization methods have been successfully developed. For instance, absolute spectra of metal clusters were determined by the method of photodepletion, where a photon absorption suffices to remove the cluster from the observed spectrum [9,10]. Similarly, the rate of photofragmentation of polyaromatic hydrocarbons [11] or the survival time of fullerene dianions in a penning trap [12] was successfully used for determining absolute photo absorption cross sections.

However, the mentioned techniques share one potential drawback: they rely on photoinduced changes of the particle composition. This may be undesirable in some situations, and it can involve ambiguities. In particular, for mass mixtures of clusters or large polymers it may occur that the mass spectrum is photodepleted towards smaller masses but simultaneously refilled from high mass compounds [13]. Although recently established transition matrix methods allow us to handle rather complex decay chains [14], it still appears desirable to develop a method that permits us to determine absolute absorption cross sections without modifying the molecule and without knowing the particle density.

The measurement scheme proposed below is based on the insight that the least invasive spectroscopic method consists in determining the momentum recoil imparted by a single photon on the flying molecule. While single-photon recoil effects have already been proposed for nonlinear spectroscopy of atoms [15], the photon momentum is usually significantly smaller than the molecular momentum spread in those classical beam experiments, so that the resulting beam broadening is hard to resolve. Modern quantum interferometers show a way around this limitation and, indeed, atom-interferometric recoil measurements have already led to precision experiments. For instance, the photon-induced recoil of neutral alkali-metal atoms allows one to determine the value of h/m_{atom}, which enters in an improved measurement of the fine structure constant α [16–18]. Optical momentum transfer was also central in investigations of photon-induced decoherence processes in matter wave interferometry [19,20] and the single-photon recoil was an essential part in Ramsey-Bordé interferometry with I_2 [21].

In the present contribution, we aim at an interferometric determination of the absolute photon absorption probability through a comparison of undeflected and deflected molecular interference patterns. We will see that near-field matter wave interferometry is particularly well suited for this purpose, since it imposes a spatial nanostructure on the traversing mo-
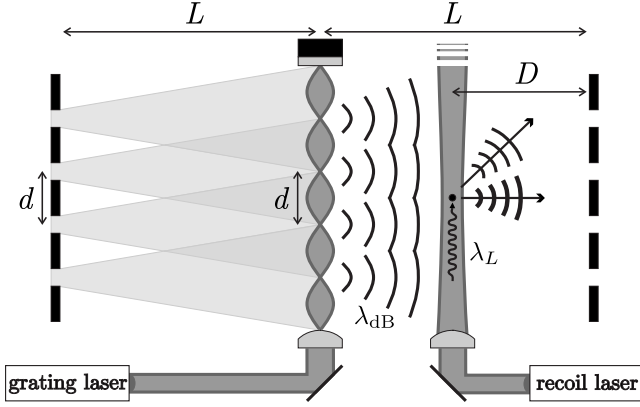
FIG. 1. Setup of the proposed measurement scheme. The molecular beam enters from the left through a material grating, and the transmitted molecules are counted after passing the grating mask on the right-hand side. In the center, a standing light field created by the grating laser serves as a diffraction element for near-field Talbot-Lau interference of the molecular matter waves. When the molecules pass the recoil laser beam they may absorb an integer number of photons, thus effecting a probabilistic modification of the interference pattern. For an appropriate choice of the distance D, the nanostructured, periodic form of the interference pattern thus enables a robust and precise extraction of the molecular absorption cross section by observing how the quantum interference contrast reduces as a function of the recoil laser power.

lecular beam [22,23] and since the interferometer fringe visibility allows us to precisely determine any changes caused by single photon recoil. After outlining the general idea, we will present a quantum theoretical description of the effect. It is sufficiently detailed to permit assessing the expected measurement accuracy in case of the photon absorption alone. In a second step, we will also account for the possible effect of fluorescence, resulting in a precise measurement scheme for both the absolute absorption cross section and for the quantum yield of fluorescence of neutral complex molecules and nanoparticles.

II. BASIC SETUP

The measurement scheme is based on the Talbot Lau interferometer (TLI), which consists of three gratings, as sketched in Fig. 1. The first and the third one are material masks, while the second diffraction element can be either an absorptive material [24] or a pure phase grating created by a standing laser wave. The latter variant, designated as the Kapitza-Dirac-Talbot-Lau configuration (KDTLI) [25], has the advantage that the power of the optical diffraction grating can be easily tuned, adding an additional handle for the experiments [26].

In the basic setup the gratings have identical grating periods d and are placed at equal distances L. A spatially incoherent, but velocity-selected molecular beam with de Broglie wave length λ_{dB} illuminates the first grating, creating the spatial coherence for diffraction at the second grating. A near field interference effect, which depends on the ratio of L to the Talbot length $L_T = d^2/\lambda_{dB}$ [27], yields a periodic density

pattern further downstream. The interference contrast depends on the wave length of the molecules, determined by their longitudinal velocity v_z, and also on the specific interactions with the diffraction structure.

The third grating serves as a transversally movable mask for a detector that measures the total molecule flux behind the gratings. The resulting fringe pattern as a function of the third grating displacement characterizes the interference pattern. Its functional form is well approximated, in both interferometer designs and under many experimental circumstances, by a simple sine curve with an offset.

We here propose to extend this arrangement by an additional recoil laser beam, running parallel to the gratings and crossing the molecular beam perpendicularly at a variable position D between the second and the third grating, as sketched in Fig. 1. Depending on the recoil laser power P_L, its wavelength λ_L, and the molecular absorption cross section σ_{abs}, each molecule may absorb one or more photons or may remain unaffected. The resulting recoils shift the associated interference patterns by an amount which depends on the distance D and on the molecular velocity v_z. The observed fringe pattern is an average of all individual molecular interference patterns, whose weights are determined by the absorption cross section. We will show in the following that the observed fringe visibility, and in particular its variation with the spectroscopy laser power, then allow one to derive a precise value for the absolute optical absorption cross section.

III. THEORETICAL ANALYSIS

The motional state of the molecules is most conveniently represented in phase space, where it is characterized by the Wigner function $w(x,p)$ of the transverse position x and momentum p with respect to a longitudinally comoving frame at fixed beam velocity v_z [28,29]. In this framework, the absorption of each individual laser photon leads to a momentum kick $\Delta p = h/\lambda_L$. The resulting fringe pattern at the third grating is then shifted by

$$s = \frac{\Delta p}{p_z} D = \frac{\lambda_{dB}}{\lambda_L} D, \tag{1}$$

where $\lambda_{dB} = h/mv_z$ is the de Broglie wavelength of the molecules. We require that the shift s be less than one grating period d in order to maintain an unambiguous assignment between the fringe shift and the absorption cross section. This limits the range of possible spectroscopy wavelengths λ_L to $\lambda_L \leqslant \lambda_{dB} L/d$, since $D < L$ (which is a minor constraint since a single wavelength is often sufficient for calibrating an entire spectrum).

The spatial density distribution at the third grating is given by an incoherent sum of the shifted distributions

$$w_3(x;n_0,s) = \sum_{n=0}^{\infty} P_n(n_0) w_3^{(0)}(x+ns), \tag{2}$$

where $w_3^{(0)}(x)$ denotes the periodic density pattern without the recoil laser. The probability $P_n(n_0)$ that a molecule absorbs n photons while crossing the laser can be modeled by a

Poissonian distribution $P_n(n_0) = n_0^n \exp(-n_0)/n!$. The average number of absorbed photons n_0 is obtained by integrating the recoil laser intensity over the longitudinal Gaussian laser profile

$$n_0 = \sqrt{\frac{2}{\pi}} \frac{\sigma_{abs} P_L \lambda_L}{hc w_y v_z}, \qquad (3)$$

where w_y is the laser waist perpendicular to the molecular beam and σ_{abs} the absorption cross section of the molecules. Here the transverse motion of the molecules through the beam can be safely neglected since the molecular beam is typically collimated to about 1 mrad [30].

The assumption of a Poissonian distribution $P_n(n_0)$ is valid if consecutive absorption processes are independent, i.e., if the cross section σ_{abs} does not change after the first excitation. In general, this cannot be taken for granted. In fact, various cases of optical limiting are known, with fullerenes as a prominent example [31]. In practice, the spectroscopy laser power shall therefore always be limited to $n_0 < 1$, leading to relaxed power requirements in the experiment.

The modified molecular density distribution (2) is determined in Fourier space by the coefficients

$$w_l(n_0, s) = w_l^{(0)} \exp\left[n_0 \exp\left(\frac{2\pi i l s}{d}\right) - n_0 \right], \qquad (4)$$

with $w_l^{(0)}$ the Fourier series coefficients of the unperturbed interference pattern $w_3^{(0)}(x) = \Sigma_l w_l^{(0)} \exp(2\pi i l x/d)$. Since the real part of the exponent in Eq. (4) is negative for $l \neq 0$ the contrast of the density pattern decreases if a recoil laser is applied, i.e., the Talbot-Lau interference blurs. This effect gets less important when the recoil laser approaches the third grating. Note that the unperturbed coefficients $w_l^{(0)}$, the recoil shift s, and the mean absorption n_0 depend on the molecular velocity, taken to be at a fixed value v_z for the time being. A finite velocity spread in the beam can be accounted for in the end by taking the average over the molecular velocity distribution.

The detected signal $S(x)$ as a function of the third grating displacement x is subject to the same transformation (4), since its Fourier coefficients S_l differ from the w_l by a multiplication with the coefficients of the transmission function of the third grating [28,29]. Our treatment assumes that the detection process is independent of the internal molecular state, which is well justified since the detection process behind the interferometer typically occurs several hundred microseconds after the excitation inside the interferometer. The incident photon energy will have been either reradiated in a fluorescence process, or will have been dissipated into many vibrational modes to which most detection mechanisms are insensitive.

It is interesting to note that one could even measure separately a possible absorption-induced change in the detection efficiency, by choosing the distance D such as to set the photon-induced shift to equal a full fringe period $s = kd$. Since this alone does not change the experimental signal,
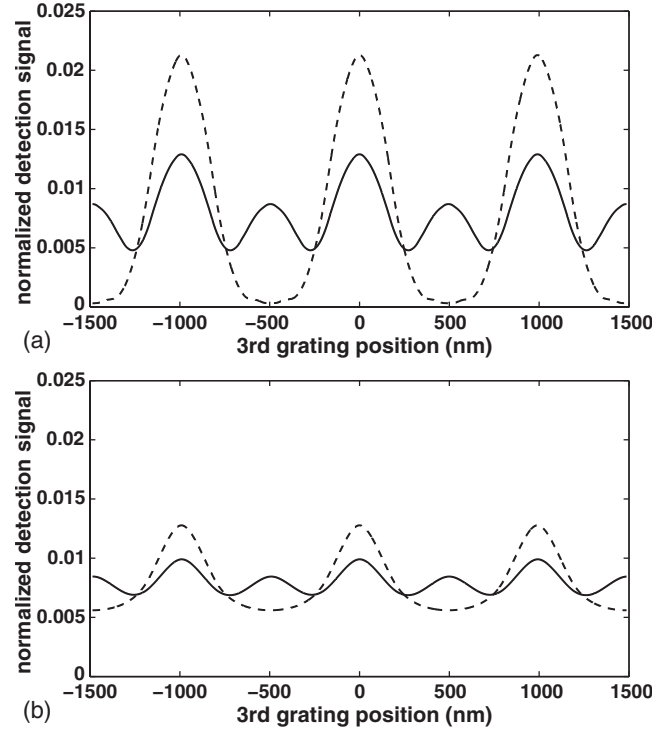

FIG. 2. Effect of a half-period recoil shift on the interference signal of a TLI setup composed of three metallic gratings with a period of 991 nm and an open fraction of $f = 1/5$, implying a slit width of $a = 198.2$ nm. The plots show the expected signal as a function of the transverse position of the third grating, normalized to the flux of the molecular beam entering the interferometer. The dashed line in panel (a) shows the peaked fringe pattern for tetraphenylporphyrin (H_2TPP) molecules passing the interferometer at fixed velocity of 175 m/s. It is changed to the solid line by a 420 nm recoil laser of 0.5 W power that shifts the pattern by half a period per absorbed photon. Panel (b) shows an analogous situation, where the molecular beam displays a Gaussian velocity distribution centered at $\bar{v}_z = 175$ m/s with a relative width of $\Delta v / \bar{v}_z = 5\%$.

additional effects related either to fluorescence effects or to photon-induced modifications of the detection efficiency thus get experimentally accessible.

The effect of the laser recoil is maximized, on the other hand, when the density pattern is shifted by half its period d per photon, i.e., by $s = (2k+1)d/2$ with integer k for a fixed molecular velocity v_z. Equation (2) then simplifies to

$$w_3\left(x; n_0, \frac{d}{2}\right) = e^{-n_0} \cosh(n_0) \left[w_3^{(0)}(x) + \tanh(n_0) w_3^{(0)}\left(x + \frac{d}{2}\right) \right],$$

$$(5)$$

where the ratio of the shifted and the unshifted pattern, given by $\tanh(n_0)$, rapidly approaches unity for $n_0 > 1$.

This special case is illustrated in Fig. 2, for a standard TLI setup with three equidistant material gratings of period $d = 991$ nm and an open slit fraction $f = a/d = 0.2$. Here and in the following examples we use the biodye tetraphenylporphyrin H_2TPP at an average velocity $\bar{v}_z = 175$ m/s. It has a mass of $m = 614.74$ amu, a static polarizability of $\alpha = 105$ Å^3 [32], and it exhibits a large optical absorption

cross section $\sigma_{abs} = 15$ Å^2 at the resonance frequency λ_L $=420$ nm [33]. This corresponds on average to $n_0 = 1.6$ absorbed photons per Watt power of the spectroscopy laser at that wavelength, when it is focused on a waist of w_y $=900$ μm, which is typical for current interferometry experiments [25].

Figure 2 shows the expected signal as a function of the third grating position when the grating distance matches exactly the Talbot length $L_T = mv_zd^2/h = 26.48$ cm. Due to the small grating slits and the fixed velocity $v_z = 175$ m/s in Fig. 2(a), one observes a fringe pattern with distinct narrow peaks (dashed line). Photoabsorption from a laser of $P = 0.5$ W positioned at $D = 5.61$ cm, generates growing side peaks shifted by half a fringe distance and reduces the magnitude of the original peak accordingly (solid line), as described by Eq. (5).

The appearance of a distinct side peak can be used as a clear indication of the recoil effect. Absolute cross sections can then be determined by comparing the side peak height to that of the original peak using Eq. (5). This concept should work very well for molecular beam sources that can be made sufficiently intense to permit a velocity selection well below 1%. This holds, in particular, for experiments that exploit laser desorption into a freely expanding seed gas jet [34].

A precise quantitative evaluation may, however, often be compromised in practice by a finite velocity spread $\Delta v_z/\bar{v}_z$ of the molecule beam, as demonstrated in Fig. 2(b). It assumes a Gaussian velocity distribution centered at $\bar{v}_z = 175$ m/s with a relative width of 5%. The interference pattern gets blurred because of the strong velocity dependence of the interference contrast of a TLI with small-slit material gratings [25,29]. The signal peaks (dashed line) therefore overlap and render the extraction of the absorption cross section inaccurate. A growing molecular mass and polarizability, as well as the possibility of fluorescence, will worsen the situation. Therefore, when precision and scalability to larger molecules matter, a tunable KDTLI laser grating setup is to be preferred to the TLI, even though the qualitative distinction of two separate sets of interference peaks gets lost.

Specifically, in case of the near-sinusoidal fringe patterns expected in a KDTLI setup [25] the recoil laser simply reduces the detected sinusoidal fringe visibility $\mathcal{V} = 2|S_1/S_0|$ by the factor

$$R(n_0, s) = \exp\left\{ -n_0\left[1 - \cos\left(\frac{2\pi s}{d}\right) \right] \right\} \quad (6)$$

according to Eq. (4). The reduction is mainly determined by the mean absorbed photon number n_0 and it can be at most $R(n_0, (2k+1)d/2) = \exp(-2n_0)$ in the case of a half-period shift. It follows with Eq. (3) that a linear relation holds between the logarithm of R and the cross section σ_{abs},

$$\ln R^{-1} = 2\sqrt{\frac{2}{\pi}} \frac{\lambda_L}{hcw_yv_z} \sigma_{abs} P_L. \quad (7)$$

One therefore easily extracts σ_{abs} from a linear regression to the measured contrast reduction for different recoil laser powers P_L. This procedure is rather robust against dephasing and contrast-reducing effects inside the interferometer, such

as grating vibrations, gravitational and Coriolis forces [35], collisions with residual gas molecules [36], or the absorption of photons at the second laser grating [25,30], since the only relevant effect is the reduction of the fringe contrast relative to the value in absence of the recoil laser.

However, this method still displays some sensitivity to the velocity spread of a realistic molecule beam. Not only the interference pattern itself depends on the longitudinal velocity v_z, but also the mean absorbed photon number (3), as well as the fringe shift (1) imparted by the recoil laser. Each Fourier component (4) of the interference pattern must therefore be averaged over a realistic velocity distribution $\mu(v_z)$. This affects the terms $w_l^{(0)}$, n_0, and s. The reduction factor (6) is then replaced by

$$\langle R \rangle_{v_z} = \left| \frac{\left\langle w_1^{(0)} \exp\left\{ -n_0\left[1 - \exp\left(\frac{2\pi is}{d}\right) \right] \right\} \right\rangle_{v_z}}{\langle w_1^{(0)} \rangle_{v_z}} \right|. \quad (8)$$

If this was used as a fitting expression to extract the cross section from the contrast reduction it would again require knowledge of the exact velocity distribution. However, this complication can be avoided even for moderate velocity spreads, as we will discuss in the following.

IV. EXPECTED ACCURACY

In our setup the molecular velocity spread is a main cause for uncertainties when extracting the absorption cross section from Eq. (7). In order to estimate the influence of the velocity spread we assume a symmetric velocity distribution $\mu(v_z)$ peaked at the value $\bar{v}_z$ with a characteristic width of Δv_z. The recoil laser is set such that the mean recoil shift amounts to one half of the grating period at $\bar{v}_z$, $\bar{s} = d/2$. It is not advisable to use larger shifts $\bar{s} = nd + d/2$, with integer n, because of their correspondingly larger variation due to the velocity spread.

For a sufficiently small relative width $\Delta v_z/\bar{v}_z$ one may expand the full expression (8) for the contrast reduction up to quadratic order in $\Delta v_z/\bar{v}_z$ and carry out the integrations to obtain

$$\frac{\Delta R}{\langle R \rangle_{v_z}} \approx 2\bar{n}_0 \left(\frac{\Delta v_z}{\bar{v}_z}\right)^2 \left(\bar{n}_0 - 1 + \frac{\pi^2}{2} + \frac{\bar{v}_z}{\bar{\mathcal{V}}_0}\frac{\partial\bar{\mathcal{V}}_0}{\partial\bar{v}_z}\right), \quad (9)$$

with $\bar{\mathcal{V}}_0$ the visibility in absence of the recoil laser and $\bar{n}_0$ the mean absorbed photon number at $\bar{v}_z$. The influence of the velocity dependence of the interference contrast $\bar{\mathcal{V}}_0$ is naturally suppressed by choosing setup parameters that maximize its value with $\partial\bar{\mathcal{V}}_0/\partial\bar{v}_z = 0$. This only holds as long as the contrast varies slowly within $\bar{v}_z \pm \Delta v_z$, which should be experimentally achievable for relative velocity spreads below 10% [25,29]. The remaining uncertainty in Eq. (9) results from the velocity dependence of the photon number n_0 and the recoil shift s. Since $n_0 \lesssim 1$ the relative error related to the velocity distribution is no more than $\Delta R/\langle R \rangle_{v_z}$ $= \pi^2 \bar{n}_0 \Delta v_z^2/\bar{v}_z^2$, which directly contributes to the systematic error $\Delta\sigma_{abs}/\sigma_{abs}$ of the derived absorption cross section, according to Eq. (7).
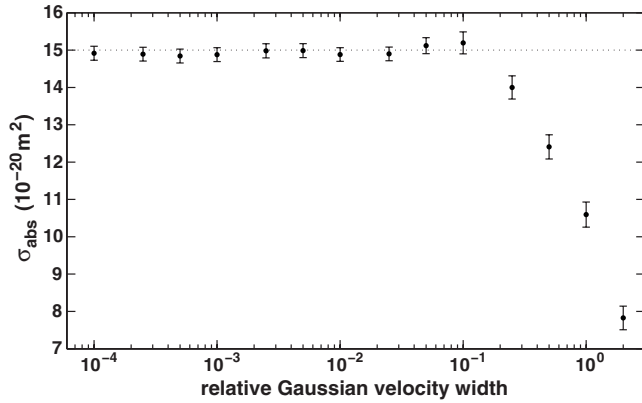
FIG. 3. Monte Carlo simulation of the proposed measurement of the absorption cross section of H_2TPP at 420 nm (see text). The results (including error bars at a 95% confidence level) are plotted versus the relative width $\Delta v_z / \bar{v}_z$ of a Gaussian velocity distribution of the molecules underlying the simulation. The dotted line marks the true value of the absorption cross section $\sigma_{abs} = 15$ Å^2 [33]. It is well reproduced by the simulated measurement for velocity spreads below 10%.

With a fair velocity selection of about 1%, which should be feasible in future experiments [34], the error can thus be reduced to 0.1%. Other experimental uncertainties, such as the power P_L and waist of the recoil laser or its distance D to the third grating, can also be reduced to the percent level.

The precision of our recoil spectroscopy method therefore hinges on a good velocity selection. This is demonstrated in Fig. 3, where we show the results of a Monte Carlo simulation of a KDTLI experiment for H_2TPP molecules. We use the setup parameters from an existing experiment [25] ($L = 10.5$ cm, $d = 266$ nm) with a grating laser power of 8 W. In this situation the velocity dependence of the interference contrast, i.e., $\partial \bar{\mathcal{V}}_0 / \partial \bar{v}_z$, can indeed be neglected in Eq. (9). The absorption of Laser grating photons is included in the simulation, with a realistic cross section of 0.17 Å^2 [33]. The 420 nm recoil laser is placed at $D = 1.51$ cm, which conforms to a recoil shift $s = d/2$ for molecules with $\bar{v}_z = 175$ m/s. Taking the velocity distribution of the molecules to be a Gaussian centered at $\bar{v}_z$, the simulation of the experiment is now done for different relative widths of the distribution in Fig. 3. Each data point represents the result of fitting Eq. (6) to a set of simulated visibilities, in which the recoil laser power is ramped up to 1 W in 20 steps. In each step the raw statistical data is given by the number of detected molecules as a function of the third grating position in a total of 100 samples over five grating periods, where each sample consists of 10^4 molecules entering the KDTLI, a value in accordance with the count rates obtained in recent experiments [25]. A sine function is then fitted to the raw data for a given recoil laser power to obtain the visibility including a statistical error estimate.

The simulation corroborates the analytical estimate that the absorption cross section (dashed line) could still be determined with a precision of about 1% provided that the molecular velocity spread can be reduced to below 10%. Above this value the velocity dependence of the signal contrast gets significant and the applied fit function (6) fails to

reproduce the correct value of the cross section. The error bars in Fig. 3 indicate the statistical uncertainty of the fringe contrast, which is mainly due to the detection shot noise and can be reduced by increasing the brilliance of the molecular beam.

The predicted accuracy of 1% is valid if other experimental parameters can be determined with that precision. This includes in particular the waist, the power and the position of the spectroscopy laser beam. Using commercially available meters it is realistic to assume these parameters to be known to better than 5%. On the one hand this accuracy would improve direct extinction measurements, where the restricted knowledge of the vapor pressure may yield uncertainties up to a factor of two [7,8]. Precision can only be gained in the rare cases where the vapor pressure of the probed molecule is large and accurately measured [4]. Our method, however, is applicable to molecular beams of low density and does not depend on the knowledge of vapor pressures.

On the other hand, our method compares favorably with the results of earlier depletion experiments [9,10,37] and electron detachment experiments [12], exhibiting errors of the order of 10%. This is due to the fact that it requires the absorption of on average less than a single soft photon only. The photon does not need to cause any fragmentation, ionization or other depletion. The probability of multiphoton absorption can be kept small, $P_{n \geq 2}(n_0) < 10\%$ for $n_0 < 0.5$, and our spectroscopic method therefore probes most particles in the same state, without any additional heating of the molecule or cluster.

V. THE EFFECT OF FLUORESCENCE

One possible side effect still remains to be considered in our discussion. Upon absorbing a photon, the molecules may either redistribute the energy in an internal conversion process or reemit the energy as a fluorescence photon, typically on the time scale of a few nanoseconds after the excitation. This can alter the reduction of the interference contrast significantly, and it would be a major source of error if it remained unconsidered. In fact, our exemplary molecule H_2TPP does fluoresce with a quantum yield of about 11% [33].

A great advantage of our near-field setup is that we can separate the side effects related to the recoil laser by varying the recoil shift within one grating period. This is due to the strict periodicity of the interference pattern, a feature absent in far field interference. As an important application of that, we can thus assess the effect of molecular fluorescence. In a simple model each photon absorption is followed by an immediate fluorescence with a probability given by the quantum yield P_{fluo}; otherwise the excitation energy is deposited in the internal state of the molecule. This assumes that the photon absorption rate during the laser passage is small compared to the inverse of the typical fluorescence time of the molecule, which is the case for typical molecules and laser powers.

Each fluorescence emission can then be treated as a single decoherence event that transforms the molecular Wigner function $w(x,p)$ to $\int dq \, \tilde{\gamma}(q) w(x, p-q)$, corresponding to a

probabilistic momentum kick with distribution $\tilde{\gamma}(q)$. The latter is given by the Fourier transform of the decoherence function [28]

$$\gamma(x) = \int_0^{\infty} d\omega F(\omega)\,\mathrm{sinc}\!\left(\frac{\omega x}{c}\right), \qquad (10)$$

where $F(\omega)$ represents the normalized fluorescence spectrum. By means of the probability $p_{n,k} = \binom{n}{k} P_{\mathrm{fluo}}^k (1 - P_{\mathrm{fluo}})^{n-k}$ of emitting k out of n absorbed photons, the Fourier coefficients of the fringe pattern can be expressed as

$$w_l(n_0, s) = w_l^{(0)} \exp\!\left(-n_0\left\{1 - \exp\!\left(\frac{2\pi i l s}{d}\right)\right.\right.$$
$$\left.\left.\times\left[P_{\mathrm{fluo}}\gamma\!\left(\frac{l\lambda_L s}{d}\right) + 1 - P_{\mathrm{fluo}}\right]\right\}\right). \qquad (11)$$

In the absence of fluorescence, $P_{\mathrm{fluo}} = 0$, expression (11) reduces to Eq. (4). The absorption cross section σ_{abs} [or equivalently the mean number n_0 of absorbed photons, according to Eq. (3)] and the quantum yield P_{fluo} can then be obtained one after the other by subsequently setting the recoil shift to $s = d/2$ and to $s = d$, and by measuring the corresponding reduction factors of the sinusoidal interference contrast

$$\ln R^{-1}\!\left(n_0, \frac{d}{2}\right) = 2n_0 - P_{\mathrm{fluo}} n_0 \left[1 - \gamma\!\left(\frac{\lambda_L}{2}\right)\right], \qquad (12)$$

$$\ln R^{-1}(n_0, d) = P_{\mathrm{fluo}} n_0 [1 - \gamma(\lambda_L)]. \qquad (13)$$

Since the latter depends only on the product $P_{\mathrm{fluo}} n_0$ it can be used to eliminate the fluorescence term in the first reduction factor. The two reduction factors together thus determine both the absorption cross section σ_{abs} and the quantum yield P_{fluo}. Note that this procedure requires knowledge of the relative fluorescence spectrum. This can, for instance, be measured close to the molecular source where the density is still high.

Figure 4 demonstrates the influence of fluorescence on the recoil-induced contrast reduction for the H_2TPP example as used in the simulation above. We plot the negative natural logarithm of the reduction factor as a function of the power of the recoil laser for three instances: The solid line depicts the situation (7) without fluorescence, as used in the simulation in Fig. 3, while the dashed and the dotted line represent the reduction factor (12) with a realistic fluorescence quantum yield of $P_{\mathrm{fluo}} = 11\%$ [33] and with the maximum value $P_{\mathrm{fluo}} = 100\%$, respectively. The underlying fluorescence spectrum is taken from [33], which evaluates the decoherence function (10) as $\gamma(\lambda_L/2) = 0.49$. One observes in Fig. 4 that the slope of the dashed line is 3% smaller than the slope of the solid line, which means that one would obtain a value for the absorption cross section σ_{abs} that is 3% too small if the fluorescence effect was ignored. Larger quantum yields lead to a more significant deviation of up to 25%, as illustrated by the dotted line.

In principle, the visibility could be additionally reduced by the recoil laser since the heating of the internal molecular
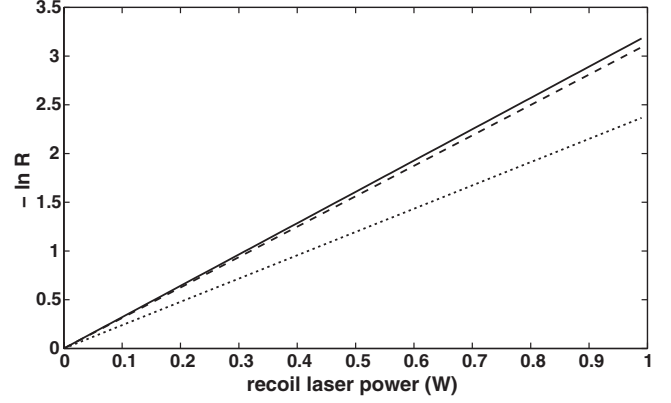

FIG. 4. Influence of fluorescence on the KDTLI contrast reduction by the recoil laser. The theoretical values of the negative logarithm of the contrast reduction factor (12) are plotted versus the power of the recoil laser for H_2TPP molecules at $v_z = 175$ m/s, with all experimental parameters the same as in Fig. 3. The solid line corresponds to the case without fluorescence, $P_{\mathrm{fluo}} = 0$, while the dashed line represents the case of a realistic quantum yield $P_{\mathrm{fluo}} = 11\%$ and the dotted line corresponds to maximally possible value $P_{\mathrm{fluo}} = 100\%$.

state can give rise to thermal emission and decoherence [28,38]. In fact, each absorbed laser photon that is not reemitted by fluorescence increases the internal temperature of the molecule by $\Delta T = hc/\lambda_L C$, with C the molecular heat capacity. However, on the time scale of the proposed experiment the enhanced thermal radiation is expected to be negligible for large molecules with capacities $C \gg k_B$, where the temperature increase per photon remains typically below 100 K for particles beyond 200 atoms [38]. Such heating effects, but also a power dependence of the absorption cross section, would manifest themselves in a nonlinear behavior of the logarithmic contrast reduction when the average number of absorbed photons is $n_0 > 1$.

Our method only measures the thermal average of the absorption cross section at a temperature given by the source. While in effusive sources this temperature could be as high as several hundred K both supersonic source and buffer gas cooled cluster sources would prepare the particles in low internal states, often the vibrational ground state.

Nevertheless, the source temperature is of particular importance for small clusters and molecules where internal heating can change the spectral properties quite dramatically [5,39–41]. While this appears to be a potential complication at first sight the optical absorption cross section can actually be a valuable probe for the cluster temperature as well [37]. And future experiments might explore this again systematically by starting from internally cold particles which are subsequently heated using laser light.

VI. CONCLUSIONS

Our analysis suggests that single photon recoil interactions within a near-field matter wave interferometer are a promising tool for absorption spectroscopy in molecular and cluster physics. The method is robust and general since it

does not depend on the particularities of the interferometer, such as the details of the molecular interaction with the diffracting element: The interferometric setup is only required to generate a fringe pattern with a good modulation of the molecular density at a sufficiently high signal-to-noise ratio.

The technique appears to be well suited for a large variety of neutral nanoparticles, including fluorescent molecules. It is particularly applicable to particles with a strong internal state conversion, a property found in many organic molecules and metal clusters.

Quantum interference experiments planned for the near-future should be capable to host a vast range of species in the mass range up to 10 000 amu, while the principle can be easily scaled to larger particles as soon as sufficiently slow and cold beams of massive particles become available. A particular advantage of the present method is that one can extract absorption cross sections from beams that are optically extremely thin. Our simulation indicates that molecular beams with densities down to $n \simeq 10^5$ cm^{-3} should already suffice. For the molecule H_2 TTP used in the example above this corresponds to an extinction length of about 65 000 km.

[1] G. Scoles, in *Atomic and Molecular Beam Methods*, edited by G. Scoles, D. Bassi, U. Buck, and D. Lainé (Oxford University Press, New York, 1988).

[2] U. Kreibig and M. Vollmer, *Optical Properties of Metal Clusters* (Springer, Berlin, 1995).

[3] J. Berkowitz, *Atomic and Molecular Photoabsorption: Absolute Total Cross Sections* (Academic Press, New York, 2002).

[4] T. Sakurai and H. G. de Winter, J. Appl. Phys. **46**, 875 (1975).

[5] F. Z. Chen, D. L. Judge, C. Y. R. Wu, and J. Caldwell, Planet. Space Sci. **47**, 261 (1998).

[6] M. G. H. Boogaarts and G. Meijer, J. Chem. Phys. **103**, 5269 (1995).

[7] P. F. Coheur, M. Carleer, and R. Colin, J. Phys. B **29**, 4987 (1996).

[8] H. Yasumatsu, T. Kondow, H. Kitagawa, K. Tabayashi, and K. Shobatake, J. Chem. Phys. **104**, 899 (1996).

[9] C. Wang, S. Pollack, D. Cameron, and M. Kappes, J. Chem. Phys. **93**, 3787 (1990).

[10] M. B. Knickelbein and W. J. C. Menezes, Phys. Rev. Lett. **69**, 1046 (1992).

[11] T. Pino, N. Boudin, and P. Bréchignac, J. Chem. Phys. **111**, 7337 (1999).

[12] B. Concina, M. Neumaier, O. Hampe, and M. M. Kappes, J. Chem. Phys. **128**, 134306 (2008).

[13] P. Brockhaus, I. V. Hertel, and C. P. Schulz, J. Chem. Phys. **110**, 393 (1999).

[14] N.-T. Van-Oanh, P. Desesquelles, and P. Brechignac, J. Phys. Chem. A **110**, 5599 (2006).

[15] J. Guo, P. R. Berman, B. Dubetsky, and G. Grynberg, Phys. Rev. A **46**, 1426 (1992).

[16] D. S. Weiss, B. C. Young, and S. Chu, Phys. Rev. Lett. **70**, 2706 (1993).

[17] S. Gupta, K. Dieckmann, Z. Hadzibabic, and D. E. Pritchard, Phys. Rev. Lett. **89**, 140401 (2002).

[18] P. Clade, E. de Mirandes, M. Cadoret, S. Guellati-Khelifa, C. Schwob, F. Nez, L. Julien, and F. Biraben, Phys. Rev. Lett. **96**, 033001 (2006).

[19] T. Pfau, S. Spälter, C. Kurtsiefer, C. R. Ekstrom, and J. Mlynek, Phys. Rev. Lett. **73**, 1223 (1994).

[20] M. S. Chapman, T. D. Hammond, A. Lenef, J. Schmiedmayer, R. A. Rubenstein, E. Smith, and D. E. Pritchard, Phys. Rev. Lett. **75**, 3783 (1995).

[21] C. Bordé, N. Courtier, F. D. Burck, A. Goncharov, and M. Gorlicki, Phys. Lett. A **188**, 187 (1994).

[22] M. Berninger, A. Stéfanov, S. Deachapunya, and M. Arndt, Phys. Rev. A **76**, 013607 (2007).

[23] L. Hackermüller, K. Hornberger, S. Gerlich, M. Gring, H. Ulbricht, and M. Arndt, Appl. Phys. B **89**, 469 (2007).

[24] B. Brezger, L. Hackermüller, S. Uttenthaler, J. Petschinka, M. Arndt, and A. Zeilinger, Phys. Rev. Lett. **88**, 100404 (2002).

[25] S. Gerlich, L. Hackermüller, K. Hornberger, A. Stibor, H. Ulbricht, M. Gring, F. Goldfarb, T. Savas, M. Müri, M. Mayor, and M. Arndt, Nat. Phys. **3**, 711 (2007).

[26] S. Gerlich, M. Gring, H. Ulbricht, K. Hornberger, J. Tüxen, M. Mayor, and M. Arndt, Angew. Chem., Int. Ed. **47**, 6195 (2008).

[27] H. F. Talbot, Philos. Mag. **9**, 401 (1836).

[28] K. Hornberger, J. E. Sipe, and M. Arndt, Phys. Rev. A **70**, 053608 (2004).

[29] S. Nimmrichter and K. Hornberger, Phys. Rev. A **78**, 023612 (2008).

[30] K. Hornberger, S. Gerlich, L. Hackermüller, M. Gring, H. Ulbricht, and M. Arndt (unpublished).

[31] J. E. Wray, K. C. Liu, C. H. Chen, W. R. Garrett, M. G. Payne, R. Goedert, and D. Templeton, Appl. Phys. Lett. **64**, 2785 (1994).

[32] S. Deachapunya, A. Stefanov, M. Berninger, H. Ulbricht, E. Reiger, N. L. Doltsinis, and M. Arndt, J. Chem. Phys. **126**, 164304 (2007).

[33] H. Du, R. Fuh, J. Li, L. Corkan, and J. Lindsey, Photochem-CAD: A Computer-Aided Design and Research Tool in Photochemistry, 1998.

[34] M. Marksteiner, G. Kiesewetter, L. Hackermüller, H. Ulbricht, and M. Arndt, Acta Phys. Hung. B **26**, 87 (2006).

[35] A. Stibor, K. Hornberger, L. Hackermüller, A. Zeilinger, and M. Arndt, Laser Phys. **15**, 10 (2005).

[36] K. Hornberger, S. Uttenthaler, B. Brezger, L. Hackermüller, M. Arndt, and A. Zeilinger, Phys. Rev. Lett. **90**, 160401 (2003).

[37] M. Schmidt, C. Ellert, W. Kronmüller, and H. Haberland,

Phys. Rev. B **59**, 10970, (1999).

[38] K. Hornberger, L. Hackermüller, and M. Arndt, Phys. Rev. A **71**, 023601 (2005).

[39] C. Ellert, M. Schmidt, C. Schmitt, T. Reiners, and H. Haber-

land, Phys. Rev. Lett. **75**, 1731 (1995).

[40] M. Moseler, H. Häkkinen, and U. Landman, Phys. Rev. Lett. **87**, 053401 (2001).

[41] G. N. Makarov, Phys. Usp. **51**, 319 (2008).